⌘ Author's Choice

© 2014 by The American Society for Biochemistry and Molecular Biology, Inc.
This paper is available on line at http://www.mcponline.org

Top-down Proteomics Reveals Concerted Reductions in Myofilament and Z-disc Protein Phosphorylation after Acute Myocardial Infarction*[S]

Ying Peng‡, Zachery R. Gregorich‡§, Santosh G. Valeja‡, Han Zhang‡, Wenxuan Cai‡§, Yi-Chen Chen¶, Huseyin Guner‡‖, Albert J. Chen‡, Denise J. Schwahn, Timothy A. Hacker‡‡, Xiaowen Liu§§¶¶, and Ying Ge‡¶‖‖‖‖**

Heart failure (HF) is a leading cause of morbidity and mortality worldwide and is most often precipitated by myocardial infarction. However, the molecular changes driving cardiac dysfunction immediately after myocardial infarction remain poorly understood. Myofilament proteins, responsible for cardiac contraction and relaxation, play critical roles in signal reception and transduction in HF. Post-translational modifications of myofilament proteins afford a mechanism for the beat-to-beat regulation of cardiac function. Thus it is of paramount importance to gain a comprehensive understanding of post-translational modifications of myofilament proteins involved in regulating early molecular events in the post-infarcted myocardium. We have developed a novel liquid chromatography–mass spectrometry-based top-down proteomics strategy to comprehensively assess the modifications of key cardiac proteins in the myofilament subproteome extracted from a minimal amount of myocardial tissue with high reproducibility and throughput. The entire procedure, including tissue homogenization, myofilament extraction, and on-line LC/MS, takes less than three hours. Notably, enabled by this novel top-down proteomics technology, we discovered a concerted significant reduction in the phosphorylation of three crucial cardiac proteins in acutely infarcted swine myocardium: cardiac troponin I and myosin regulatory light chain of the myofilaments and, unexpectedly, enigma homolog isoform 2 (ENH2) of the Z-disc. Furthermore, top-down MS allowed us to comprehensively sequence these proteins and pinpoint their phosphorylation sites. For the first time, we have characterized the sequence of ENH2 and identified it as a phosphoprotein. ENH2 is localized at the Z-disc, which has been increasingly recognized for its role as a nodal point in cardiac signaling. Thus our proteomics discovery opens up new avenues for the investigation of concerted signaling between myofilament and Z-disc in the early molecular events that contribute to cardiac dysfunction and progression to HF. ***Molecular & Cellular Proteomics 13: 10.1074/mcp.M114.040675, 2752–2764, 2014.***

Despite recent advances in the treatment of heart failure (HF),[1] this devastating syndrome remains a leading cause of morbidity and mortality worldwide and imposes a significant economic burden, especially on developed countries (1–3). The most common cause of HF, myocardial infarction (MI), induces left ventricular (LV) remodeling characterized by chamber dilation and hypertrophy of the non-infarcted (re-

From the ‡Department of Cell and Regenerative Biology, University of Wisconsin-Madison, 1300 University Ave., Madison, Wisconsin 53706; §Molecular Pharmacology Training Program, University of Wisconsin-Madison, 1300 University Ave., Madison, Wisconsin 53706; ¶Department of Chemistry, University of Wisconsin-Madison, 1300 University Ave., Madison, Wisconsin 53706; ‖Human Proteomics Program, University of Wisconsin-Madison, 1300 University Ave., Madison, Wisconsin 53706; **Research Animal Resources Center, University of Wisconsin-Madison, 1300 University Ave., Madison, Wisconsin 53706; ‡‡Department of Medicine, University of Wisconsin-Madison, 1300 University Ave., Madison, Wisconsin 53706; §§Department of BioHealth Informatics, Indiana University-Purdue University Indianapolis, 719 Indiana Ave., Indianapolis, Indiana 46202; ¶¶Center for Computational Biology and Bioinformatics, Indiana University School of Medicine, 410 West 10th Street, Indianapolis, Indiana 46202

⌘ *Author's Choice*—Final version full access.

Received April 24, 2014, and in revised form, May 28, 2014

Published, MCP Papers in Press, June 26, 2014, DOI 10.1074/mcp.M114.040675

Author contributions: Y.P., T.A.H., and Y.G. designed research; Y.P., Z.R.G., S.G.V., H.Z., W.C., Y.C., A.J.C., and T.A.H. performed research; Y.P., Z.R.G., S.G.V., H.Z., W.C., Y.C., H.G., D.J.S., T.A.H., X.L., and Y.G. analyzed data; Y.P., Z.R.G., S.G.V., H.Z., W.C., Y.C., D.J.S., T.A.H., X.L., and Y.G. wrote the paper.

[1] The abbreviations used are: HF, heart failure; MI, myocardial infarction; LV, left ventricular; Tn, troponin; TnI, troponin I; TnT, troponin T; TnC, troponin C; Tm, tropomyosin; MLC2, myosin regulatory light chain; AMI, acute myocardial infarction; cTnI, cardiac troponin I; ENH2, enigma homolog isoform 2; LAD, left anterior descending; CON, control; PKA, cAMP-dependent protein kinase A; PTM, post-translational modification; MS/MS, tandem mass spectrometry; CAD, collisionally activated dissociation; ECD, electron capture dissociation; LC/MS, liquid chromatography–mass spectrometry; FT-ICR, Fourier transform ion cyclotron resonance; M_r, molecular weight; PV, pressure volume.

mote) myocardium, which is ultimately maladaptive, leading to depressed global contractility and predisposing the heart to failure (4). Current treatments for HF have primarily focused on symptom management after the occurrence of irreversible remodeling and functional impairment, which only delays the syndrome (1). Understanding the molecular mechanisms driving cardiac dysfunction at the early stages could enable the development of therapeutic interventions to prevent the onset of HF. However, the molecular changes that occur immediately after MI but prior to the maladaptive remodeling remain poorly understood (5).

Myofilaments are responsible for cardiac contraction and relaxation and play a central role in myocardial pathophysiology (6, 7). Moreover, recent evidence suggests that cardiac myofilaments have a critical role in signal reception and transduction in HF (8, 9). Myofilaments consist of thin filament proteins, which include actin, tropomyosin (Tm), and the troponin (Tn) complex (TnI, TnT, and TnC), and thick filament proteins including myosin (S-1 head domain, S-2 rod domain, essential light chain, and regulatory light chain (MLC2)), as well as a number of accessory proteins such as myosin binding protein C (6, 10–12). In addition to these major myofilament proteins, a significant number of proteins have been identified in the cardiac myofilament subproteome (13). Cardiac contraction requires the integrated activity of highly coordinated protein–protein interactions among myofilament proteins in the sarcomere (6, 8, 9). Post-translational modifications (PTMs) and mutations of myofilament proteins can change these protein–protein interactions, thereby altering cardiac contractility. Thus, it is of paramount importance to gain a comprehensive understanding of the PTM changes of myofilament proteins in the regulation of early molecular events in contractile dysfunction immediately after acute myocardial infarction (AMI).

Top-down mass spectrometry (MS) (12, 14–22) has unique advantages for the comprehensive assessment of protein modifications through the detection and quantification of all proteoforms (a unified term used to define all of the different molecular forms arising from PTMs, mutations or polymorphisms, and alternative splicing events (23)). Subsequently, the modification sites can be precisely localized via MS/MS including but not limited to collisionally activated dissociation (CAD) and electron capture dissociation (ECD) (12, 14–22, 24, 25). We have successfully developed a novel liquid chromatography–mass spectrometry (LC/MS)-based top-down quantitative proteomics strategy to assess the concerted changes in myofilaments and their associated proteins in the myofilament subproteome. Specifically, we have rapidly separated and quantified intact proteins extracted from a minimal amount of myocardial tissue (~500 μg of tissue per experiment) by means of LC/MS with high reproducibility and throughput. Notably, we discovered a concerted significant reduction in the phosphorylation of three crucial cardiac proteins in acutely infarcted myocardium using a clinically relevant swine AMI model (26): a thin filament regulatory protein, cardiac TnI (cTnI); a thick filament regulatory protein, MLC2; and, unexpectedly, a critical Z-disc protein, enigma homolog isoform 2 (ENH2). Subsequently, we unambiguously localized the phosphorylation sites of these three important proteins using ECD. Particularly, for the first time, we comprehensively sequenced swine ENH2 by means of top-down MS and identified it as a phosphoprotein with its phosphorylation site precisely pinpointed. ENH2 belongs to the PDZ-LIM protein family that co-localizes with α-actinin at the Z-disc (27, 28). Although traditionally viewed as a structural component in the sarcomere, the Z-disc is increasingly recognized for its prominent role as a nodal point for cardiac signaling (27, 29, 30). Thus, our proteomic discovery opens up new avenues for investigations of the concerted signaling between myofilament and Z-disc proteins in the early molecular events that may contribute to cardiac dysfunction and subsequent HF.

EXPERIMENTAL PROCEDURES

Generation and Functional Characterization of Swine AMI Model—We induced AMI in swine via occlusion of the left anterior descending coronary artery using an angioplasty balloon and a percutaneous femoral approach similar to that reported previously (26) (Fig. 1*A*). Briefly, Yorkshire swine (30 to 35 kg) from the University of Wisconsin-Madison colony were pre-medicated with a mixture of telazol (4 to 6 mg/kg, intramuscular), xylazine (2 mg/kg, intramuscular), and propofol (2 to 8 mg/kg, intravenous), intubated, anesthetized, and mechanically ventilated with isoflurane (1% to 5%). Baseline pressure volume (PV) loops were obtained, and the vena cava balloon was briefly inflated to alter loading conditions with the ventilator turned off. Next, a coronary balloon catheter was introduced into the proximal LAD just distal to the first diagonal arterial branch and inflated for 90 min (AMI group, $n = 6$). Iodinated contrast was used to confirm complete cessation of coronary blood flow distal to the balloon. After 90 min, PV loop data were again collected with the catheter in place and the LAD still occluded. PV analysis was performed in control animals (CON group, $n = 6$). After the final PV loop was obtained, the animal was euthanized with saturated KCl and the heart was removed and sectioned. Sections were either rapidly frozen in liquid nitrogen or placed in 10% buffered formalin for histology. 90-min occlusion of the lower one-third of the LAD created an ischemic zone including roughly 25% of the left ventricle, less than 5% of the right ventricle, and 5% to 10% of the interventricular septum. All experiments involving animals were conducted in accordance with the NIH Guide for the Care and Use of Laboratory Animals and using protocols approved by the University of Wisconsin Institutional Animal Care and Use Committee.

Histopathologic Analysis—Formalin-fixed heart sections were trimmed, processed, embedded in paraffin, cut 5 μm thick, and stained with hematoxylin and eosin (H&E) or phosphotungstic acid–hematoxylin. Staining with H&E employed routine methods, and phosphotungstic acid–hematoxylin staining was performed using Bouin solution as a mordant instead of Zenker fixative, followed by Gram iodine, sodium thiosulfate, potassium permanganate, and oxalic treatments before phosphotungstic acid–hematoxylin staining overnight.

Tissue Homogenization and Myofilament Protein Extraction—Myofilament subproteome was effectively extracted from only ~5 mg of pig myocardial tissue, which was sufficient for 10 experiments (the equivalent of 500 μg per experiment). We chose to use ~5 mg because of the difficulty associated with handling and accurately

measuring 500 μg of tissue. Specifically, ~5 mg of swine cardiac tissue was homogenized in 50 μl of HEPES extraction buffer containing protease and phosphatase inhibitors (25 mM HEPES, pH 7.5, 50 mM NaF, 0.25 mM Na_3VO_4, 0.25 mM PMSF, 2.5 mM EDTA) using a Teflon pestle (1.5-ml tube rounded tip, Cienceware, Pequannock, NJ) to remove soluble cytoplasmic proteins. The resulting homogenate was centrifuged at 16,100 rcf for 15 min at 4 °C (Centrifuge 5415R, Eppendorf, Hamburg, Germany), and the supernatant was discarded. The insoluble pellet was then re-homogenized in 50 μl of TFA extraction buffer (1% TFA, 1 mM TCEP) to extract the myofilament proteins (31). After centrifugation (16,100 rcf, 4 °C, 25 min), the supernatant, which was enriched in myofilament proteins, was collected and analyzed using LC/MS (the pellet was discarded). All tissue preparation and protein extraction procedures were performed in a cold room (4 °C) or on ice using freshly prepared buffers.

On-line LC/MS Analysis—Rapid LC/MS profiling was performed using a 2D-nanoLC system (Eksigent®, Dublin, CA) coupled on-line with a linear ion trap (LTQ)/MS system (Thermo Scientific Inc., Bremen, Germany). Samples (equivalent to ~500 μg of tissue per injection) were loaded onto a sample loop (10 μl) before a home-packed PLRP column (200 mm × 500 μm, PLRP, 10 μm, 1000 Å) with a flow rate of 12.5 μl/min. The packing material (PLRP-S particles) was purchased from Varian (Lake Forest, CA). The proteins of interest were eluted with a gradient (12.5 μl/min) of 20% B to 90% B in 55 min (solvent A: 0.15% formic acid in water; solvent B: 0.15% formic acid in methanol). After LC separation, a small portion of the sample (~5% of the total amount) was ionized by electrospray ionization through a 25-μm to 30-μm inner diameter tip and analyzed directly via LTQ/MS (on-line LC/MS). The remaining ~95% of the sample was simultaneously collected on ice for further high-resolution MS and MS/MS characterization (see below). 22 fractions were collected during one LC/MS experiment per injection (Fig. 2*B*).

Off-line High-resolution FT-ICR MS/MS Analysis—The collected fractions were analyzed using a 7T linear ion trap/Fourier transform ion cyclotron resonance (FT-ICR) mass spectrometer (LTQ/FT Ultra, Thermo Scientific Inc.) equipped with an automated chip-based nano-electrospray ionization source (Triversa NanoMate, Advion Bioscience, Ithaca, NY) as described previously (21, 32, 33). The sample was introduced into the mass spectrometer using a spray voltage of 1.3 to 1.5 kV, resulting in a flow rate of 50 to 200 nL/min. Ion transmission into the linear trap and, subsequently, the FT-ICR cell was optimized for a maximum ion signal. The resolving power of the FT-ICR was set at 200,000 at 400 *m/z*, which resulted in an acquisition rate of 1 scan per second. The numbers of accumulated ions for a full scan in the linear trap, FT-ICR cell, MS^n FT-ICR cell, and ECD were 3×10^4, 8×10^6, 8×10^6, and 8×10^6, respectively. For MS/MS experiments, the protein molecular ions of the individual charge states were first isolated and then fragmented using 15% to 20% normalized collision energy for CAD or 2.5% to 3.5% electron energy for ECD (corresponding to 1.3 to 2.3 eV) with a 70-ms duration without additional delay. All MS and MS/MS spectra were analyzed using in-house-developed MASH Suite software (version 1.0) (34) using the THRASH algorithm with a signal-to-noise ratio threshold of 3 and a minimum fit of 60%. The resulting data were then manually validated to ensure their accuracy. The most abundant mass is reported for intact proteins, whereas the monoisotopic mass is reported for fragment ions.

Protein Identification—The raw MS/MS data were converted to mzXML files and deconvoluted with MS-Deconv (release version 0.8.0) (35), a combinatorial algorithm that determines the monoisotopic mass and charge for all of the fragment ions present in an MS/MS spectrum. Subsequently, to identify the proteins present in the sample, the files containing the monoisotopic mass, intensity, and charge for each of the product ions were searched against the pig database generated by NCBI (Sscrofa10.2, containing 24,476 protein sequences) using the MS-Align+ search engine (release version 0.7.1) (36). Here, 10-ppm mass measurement accuracy was utilized as a cutoff for MS/MS fragment assignments. The maximum number of unexpected changes was two, and the acceptance criterion was an E-value less than 0.01. The use of both CAD and ECD MS/MS spectra for various charge states of the same protein resulted in unique protein identification with significantly lower statistical *p* values and a higher number of assigned fragments correlating directly to a higher confidence level in protein identification. All protein identifications were validated manually. Moreover, MS-Align+ is a fast algorithm for top-down protein identification based on spectral alignment that allows for the identification of sequence variations and PTMs, as described previously (20, 36).

Quantitative Analysis—We have quantitatively determined the proteoforms of major myofilament and associated proteins using both low-resolution LTQ/MS and high-resolution FT-ICR/MS data. For low-resolution MS data, the areas under the MS peaks were used to quantify the relative abundances of proteoforms. For high-resolution MS data, the sum of the peak heights of the top five isotopomers for each proteoform was used to calculate the relative abundance, as described previously (21, 32, 33, 37). The relative abundances of the individual proteoforms from three separate charge states were averaged to obtain the relative percentage for each individual proteoform. To assess protein phosphorylation levels, the percentages of the monophosphorylated ($\%P_{mono}$) and/or bisphosphorylated ($\%P_{bis}$) protein species were defined as the summed abundances of monophosphorylated and/or bisphosphorylated species over the summed abundances of the entire protein population, respectively. Based on these percentages, the total amount of phosphorylation (P_{total}) of a single protein was calculated using Eq. 1.

$$P_{total} = (\%P_{mono} + 2 \times \%P_{bis})/100 \qquad \text{(Eq. 1)}$$

Minor oxidation products and non-covalent phosphoric acid adducts ($+H_3PO_4$) were taken into consideration in the quantification.

Statistical Analysis—Data are represented as the mean ± S.E. Each biological replicate was performed in two technical replicates. Student's *t* test was performed between group comparisons to evaluate the statistical significance of variance. Differences among means were considered significant at $p < 0.05$.

RESULTS

A Clinically Relevant Swine AMI Model—Owing to the anatomical and physiological similarities between human and swine hearts, the swine AMI model is of high clinical relevance, as it closely recapitulates human disease pathophysiology (38). In this study, we generated a swine AMI model using a closed-chest catheter-based method (26) by inducing AMI in pigs ($n = 6$) via occlusion of the lower one-third of the LAD with an angioplasty balloon (Fig. 1*A*). Control animals (CON, $n = 6$) were treated similarly, but without LAD balloon catheterization. We chose a 90-min occlusion to mimic the typical time interval between the onset of chest pain in patients and their arrival in the emergency room for medical treatment (39). PV analysis was performed to assess cardiac function prior to and after LAD occlusion in swine undergoing AMI and prior to sacrifice in CON (Fig. 1*B*). In CON and AMI swine, prior to LAD occlusion, the heart rate, end systolic pressure, stroke volume, LV ejection fraction, and pre-load recruitable stroke work were consistent with the values pre-

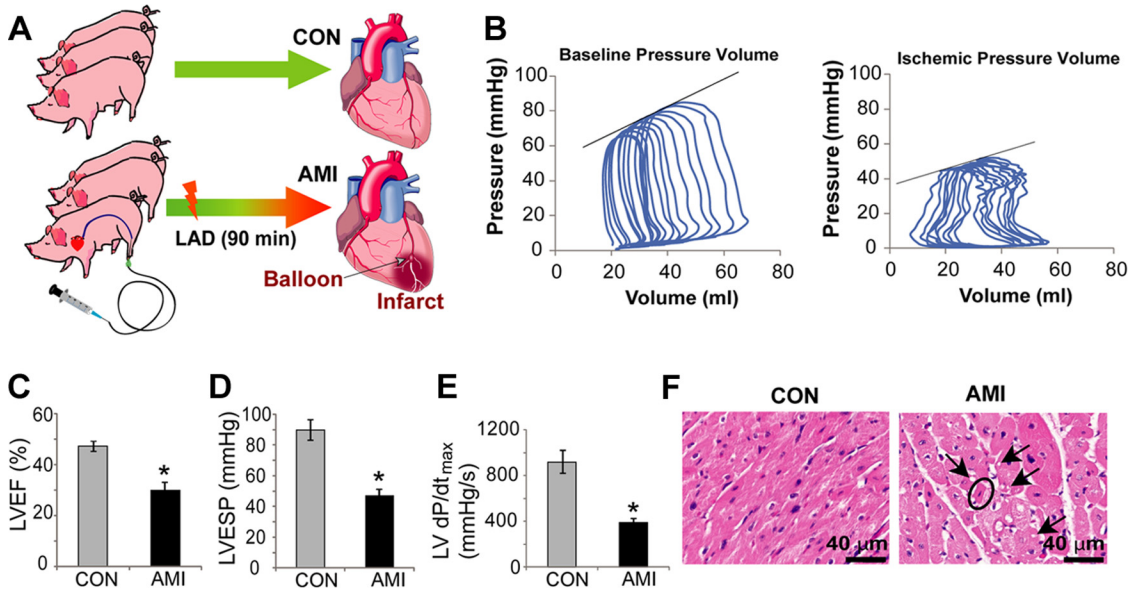

FIG. 1. **Generation and characterization of swine AMI model.** *A*, schematic of the creation of the AMI swine model *versus* CON. Tissue used in this study was from the area labeled "infarct" in AMI, whereas LV tissue was used in CON. *B*, PV measurements prior to (*left*) and after (*right*) 90 min of LAD occlusion. The slope of the straight line represents the end systolic pressure–volume relation. The flatter slope in the right-hand panel reflects a reduction in cardiac function due to ischemia. *C*, LV ejection fraction (EF) is reduced in AMI relative to CON commensurate with the reduction in blood flow. *D*, LV end systolic pressure is lower in AMI because of the lack of blood flow. *E*, LV *dP/dt*, a measure of systolic performance, is also significantly reduced for AMI swine relative to CON. *F*, H&E-stained LV tissue from CON (*left*) and AMI (*right*) pigs. Arrows denote myocyte vacuolation, and the circled cell displays characteristics consistent with necrosis, including cellular shrinkage, cytoplasmic hypereosinophilia, and nuclear pyknosis. CON, control; AMI, acute myocardial infarction; LV, left ventricular; PV, pressure volume; LAD, left anterior descending coronary artery; ESP, end systolic pressure; EF, ejection fraction; *dP/dt*, first derivative of LV pressure.

viously reported for healthy swine (supplemental Table S1) (26). After 90 min of LAD occlusion, a significant decrease in the end systolic pressure, the maximal rate of change in the pressure (dP/dt_{max}), the minimal rate of change in the pressure (dP/dt_{min}), the LV ejection fraction, and the pre-load recruitable stroke work (Figs. 1*C*–1*E*; supplemental Table S1) was observed.

Although the histological characterization of AMI is difficult because tissue necrosis only becomes readily apparent 4 to 6 h after infarction, analysis of tissue collected from the left ventricle and interventricular septum was undertaken to examine for early degenerative changes. Tissue taken from the left ventricle and interventricular septum of infarcted swine showed signs of early stage myocardial injury and necrosis (Fig. 1*F*, supplemental Fig. S1). Scattered areas of sarcomere fragmentation were most common, followed by vacuolar degeneration (Fig. 1*F*), contraction banding (supplemental Fig. S1), and shrunken cells exhibiting cytoplasmic hypereosinophilia and pyknosis (necrosis) (Fig. 1, supplemental Fig. S1). These results are consistent with the characteristics of AMI in swine.

An Integrated Top-down Quantitative Proteomics Strategy—We have developed a top-down LC/MS-based proteomics strategy for the separation, identification, quantification, and characterization of intact proteins from tissue extracts to reveal disease-related changes (Fig. 2*A*). Using this strategy, we can rapidly extract, separate, and identify intact myofilament proteins from a minimal amount of myocardial tissue (~500 μg of tissue per LC injection). It takes less than three hours to perform tissue homogenization, myofilament extraction, and on-line LC/MS analysis. We effectively separated a number of myofilament and associated proteins (Fig. 2*B*). Rapid profiling via low-resolution linear ion trap (LTQ)/MS, concurrent with LC separation, allowed for the preliminary identification of myofilament proteins based on their deconvoluted molecular masses, which matched closely with the predicted sequence in the Swiss-Prot database (Fig. 2*B*, supplemental Fig. S2, supplemental Table S2). Meanwhile, the off-line high-resolution MS analysis of the collected fractions from LC separation enabled the determination of the accurate relative molecular masses (M_r) of all of the detected proteoforms (supplemental Fig. S2). Subsequent high-resolution MS/MS together with the MS-Align+ algorithm (36) provided unambiguous identification of major proteins present in the myofilament subproteome (supplemental Table S2, supplemental Fig. S3, and supplementary text). Both low-resolution and high-resolution MS have been used for relative quantification (see below).

Quantification of Phosphorylation Using On-line LC/MS—The high reproducibility of the LC/MS experiments (supplemental Figs. S4 and S5) allowed rapid semi-quantification of proteoform abundances based on their peak areas. To ensure

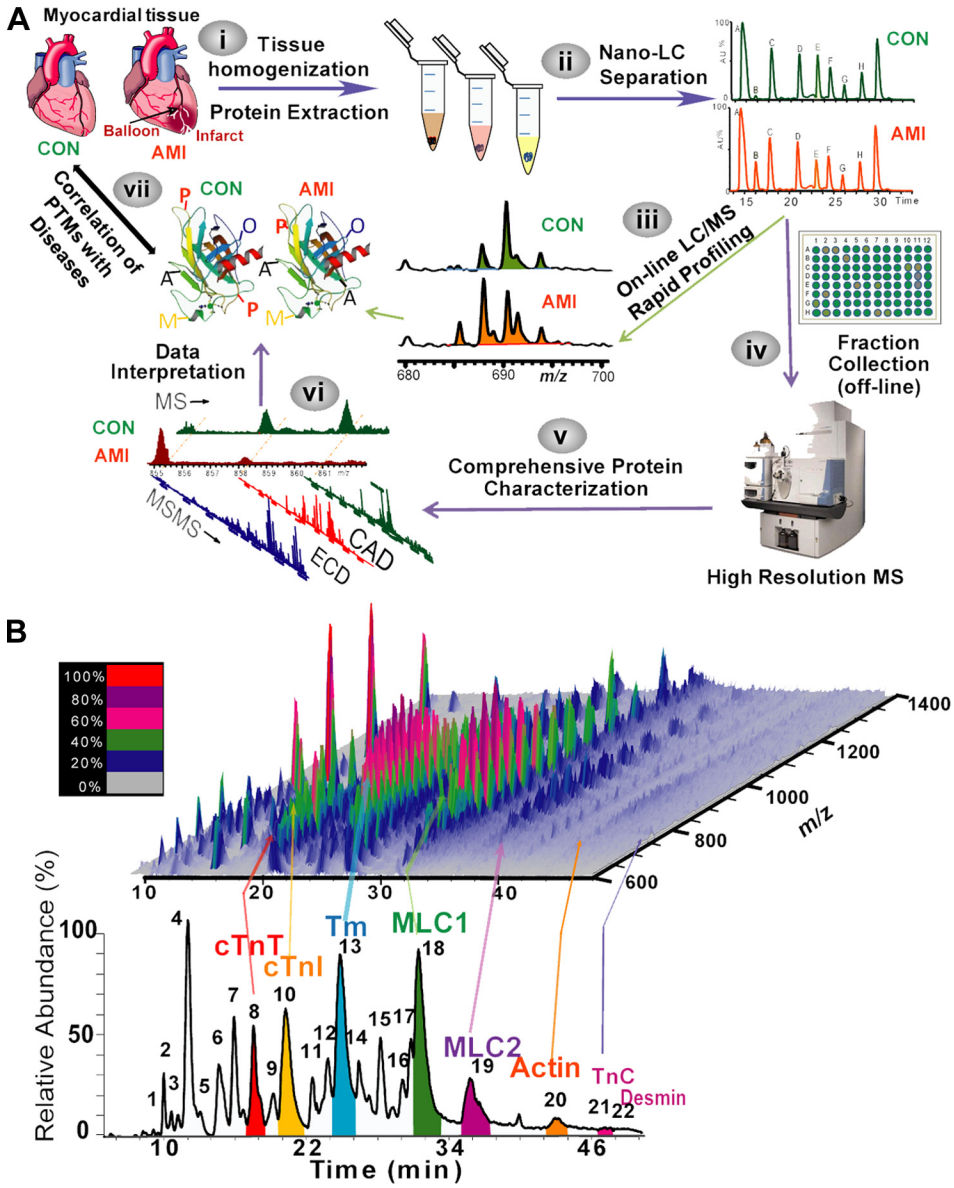

FIG. 2. *A*, schematic of the integrated top-down LC/MS-based quantitative proteomics strategy. This strategy consists of six steps: (i) tissue homogenization and protein extraction at low temperature (4 °C) in HEPES and TFA solutions containing protease and phosphatase inhibitors to preserve endogenous modifications and minimize artifactual degradations; (ii) on-line separation of proteins via nano-LC; (iii) rapid LC/MS profiling using low-resolution LTQ/MS (on-line); (iv) fraction collection concurrent with on-line LC/MS analysis; (v) comprehensive top-down MS analysis using high-resolution FT-ICR/MS (off-line); (vi) data interpretation; and (vii) correlation of proteoform changes with disease phenotype. *B*, on-line LC/MS separation and detection of swine myofilament and associated proteins. *Bottom*, LC separation of myofilament and associated proteins. The identification of each labeled peak is shown in supplemental Table S2. *Top*, on-line MS detection of the myofilament and associated proteins.

an accurate comparison, we paired AMI and CON groups and performed the LC/MS back to back using the same experimental setup (Figs. 3*A* and 3*B*, supplemental Fig. S6). Despite the limited resolution of LTQ, we were able to preliminarily identify protein phosphorylation based on the mass difference of 80 Da. Quantification of the phosphorylation of myofilament and associated proteins revealed a significant reduction in the phosphorylation of cTnI (a thin filament regulatory protein), MLC2 (a thick filament regulatory protein), and ENH2 (a Z-disc protein) in the myocardium of AMI *versus* CON, whereas no significant changes were observed in the phosphorylation levels of cardiac TnT and Tm (Fig. 3 and supplementary text). The total phosphorylation level (P_{total}, mol Pi/mol protein) of cTnI was significantly reduced from 1.72 ± 0.05 in CON to 0.97 ± 0.16 in AMI; the P_{total} of MLC2 decreased from 0.11 ± 0.01 to 0.09 ± 0.01, and the P_{total} of ENH2 decreased from 0.93 ± 0.02 in CON to 0.57 ± 0.09 in AMI (Fig. 3*C*). Collectively, these results suggest that the phosphorylation of cTnI,

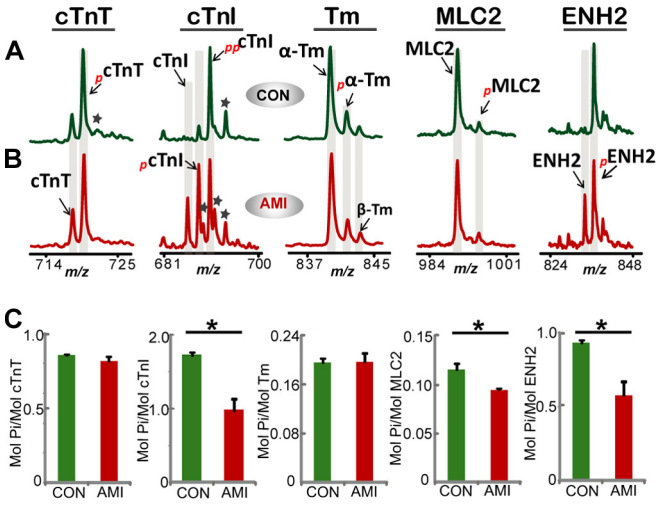

FIG. 3. **Relative quantification of phosphorylation in myofilament and associated protein from CON and AMI swine myocardium.** Representative low-resolution MS spectra showing cardiac TnT, cTnI, Tm, MLC2, and ENH2 from CON (*A*) and AMI (*B*) myocardium. The total amount of phosphorylation of cardiac TnT, cTnI, Tm, MLC2, and ENH2 is shown in *C*. All measurements were performed on three animals per group. Each biological replicate was performed in two technical replicates. The data are represented as the mean peak area ± S.E. *$p < 0.05$. Monophosphorylated and bisphosphorylated proteins are labeled with subscripts "*p*" and "*pp*," respectively. Asterisks indicate non-covalent phosphoric acid adducts.

MLC2, and ENH2 is down-regulated in the acutely infarcted myocardium.

Comprehensive Proteoform Assessment Using High-resolution MS/MS—The amalgamation of different proteoforms into a single peak in low-resolution spectra can potentially compromise the accuracy of proteoform quantification; therefore, a more accurate quantification based on high-resolution MS is necessary. High-resolution FT-ICR/MS analysis allowed a complete view of all types of proteoforms, including those arising as a result of PTM (*e.g.* phosphorylation), alternative splicing events (*e.g.* α-Tm and β-Tm), and polymorphisms (*e.g.* Tm Pro64Leu) (representative data for cTnI, MLC2, Tm, and ENH2 are shown in Fig. 4; details in supplementary text). A number of minor proteoforms that could not be identified in the low-resolution spectra were resolved in the high-resolution MS spectra (Figs. 4*A*–4*D*). Subsequently, we quantitatively determined the relative percentages of each proteoform in the corresponding gene product group (Fig. 4*E* and supplementary text). Consistent with the low-resolution MS results (Fig. 3), we observed significantly reduced phosphorylation of cTnI, MLC2, and ENH2 from AMI myocardium relative to that from the CON group (Fig. 4, supplemental Figs. S7 and S8). Additionally, dENH2 (likely a truncated form of ENH2) was up-regulated in AMI *versus* CON, but the low abundance of this proteoform hindered further MS/MS characterization. No significant differences were observed in the relative amounts of Tm proteoforms in AMI *versus* CON (Fig. 4*E*, supplemental Figs. S7 and S8).

Mapping Phosphorylation Sites in Swine cTnI to Ser22/23—cTnI is the inhibitory subunit of Tn, interacting with TnC, cardiac TnT, and actin to inhibit muscle contraction (11). Phosphorylation of cTnI is particularly important in modulating cardiac function (9, 40). Because a number of kinases can phosphorylate different sites within cTnI (40–42), it is imperative to determine which sites are modified in AMI hearts. To identify the phosphorylation sites in swine cTnI, the precursor ions of monophosphorylated cTnI ($_p$cTnI) and bisphosphorylated cTnI ($_{pp}$cTnI) were cleanly isolated and subsequently fragmented by ECD (supplemental Fig. S10, Fig. 5*A*). We comprehensively sequenced $_p$cTnI and $_{pp}$cTnI and unambiguously mapped Ser22 as the only phosphorylation site in $_p$cTnI and Ser22/23 as the two phosphorylation sites in $_{pp}$cTnI in AMI hearts (supplemental Fig. S10, Fig. 5*A*, and supplementary text). Interestingly, the fact that phosphorylation of Ser23 was only observed in the presence of Ser22 phosphorylation suggests a sequential phosphorylation mechanism, which is consistent with our previous report on human cTnI (33). Ser22/23 are *bona fide* substrates of cAMP-dependent protein kinase A (PKA), although protein kinase C (PKC), protein kinase D (PKD), and cGMP-dependent protein kinase can also cross-phosphorylate these two sites (40).

Comprehensive Sequencing and Phosphorylation Site Mapping in Swine MLC2 to Ser14—Although thin filament proteins are well recognized as critical elements regulating force production in cardiac muscle, recent compelling evidence suggests that thick filament regulatory proteins are also important players in modulating muscle contractions (43). MLC2 is a thick filament regulatory protein that is believed to function as a mechanical stabilizer for the neck region between the myosin head (S1) and rod (S2) during force generation and mechanical work performance (44). Here, we found that MLC2 was present in both unphosphorylated and monophosphorylated ($_p$MLC2) forms, with M_r values of 18,801.45 and 18,881.41, respectively (Fig. 4*B*). The M_r of unphosphorylated MLC2 matched best with the uncharacterized sequence of swine MLC2 (UniProtKB/Swiss-Prot, F6PSL2_PIG) after considering acetylation at the N-terminus. Because this sequence is not yet verified, we employed top-down MS/MS to comprehensively sequence both unphosphorylated and monophosphorylated MLC2 (supplemental Fig. S11, Fig. 5*B*). For MLC2, a total of 51 *b* ions, 52 *y* ions, 129 *c* ions, and 131 *z*· ions were detected based on seven ECD and three CAD spectra, representing 158 out of 164 bond cleavages (supplemental Fig. S11). For $_p$MLC2, 84 *c* ions and 85 *z*· ions were detected, representing 134 out of 164 bond cleavages, which unambiguously revealed that Ser14 was the predominant phosphorylation site in swine $_p$MLC2 (Fig. 5*B*, supplemental Fig. S12).

Top-down MS Uncovered Ser118 as a Phosphorylation Site in ENH2—ENH2 belongs to the PDZ-LIM protein family that co-localizes with α-actinin at the Z-disc and associates with cytoskeletal proteins through its PDZ domain (27, 28, 45).

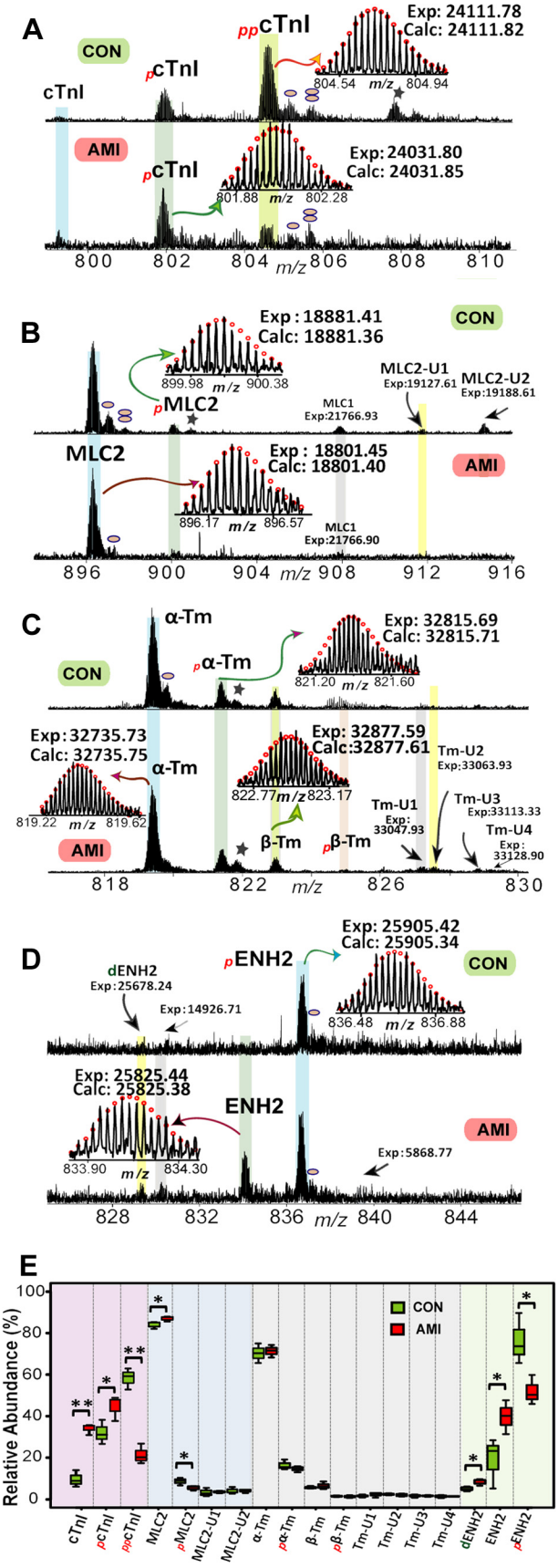

ENH2 is a short, alternatively spliced isoform of ENH that only retains the PDZ domain (27, 28, 45). Given that ENH2 phosphorylation has not been reported previously and that the phosphorylation of this protein is altered following AMI, we sought to identify the site of phosphorylation. Two major proteoforms of ENH2 were detected with M_r values of 25,825.44 and 25,905.42 (Fig. 4*D*). The mass difference of 79.98 Da between these two proteoforms implies a likely phosphorylation event. However, neither of these M_r values matched with the predicted M_r of 25,898.43, based on the predicted swine ENH2 sequence from the NCBI pig genomic database (Sscrofa10.2). Using the MS-Align+ algorithm, we identified a modification of 15 Da between Gly60 and Lys70 (supplemental Fig. S3*E*). A sequence homology alignment of the predicted swine, human, and mouse ENH2 sequences revealed a potential amino acid polymorphism of Ser72Cys (+15.98 Da) among these species (supplemental Fig. S13). Thus, considering a single amino acid polymorphism (+15.98 Da), removal of N-terminal Met (−131.04 Da), and acetylation of the new N terminus (+42.01 Da), the re-calculated M_r of swine ENH2 is 25,825.38, which matches well with the observed M_r of 25,825.44 (2.3 ppm).

To further characterize the sequence and locate the phosphorylation site of swine ENH2, we isolated the precursor ion of monophosphorylated ENH2 ($_p$ENH2) and then fragmented it via ECD. In five combined ECD spectra of $_p$ENH2, 58 *c* ions and 71 *z*· ions were detected, representing 98 out of 232 bond cleavages (Fig. 5*C*), despite the relatively lower quantity of ENH2 present in the myofilament extract (supplemental Fig. S6). The MS/MS data unequivocally validated the removal of the N-terminal Met, acetylation of the new N terminus, and one amino acid polymorphism at Ser72Cys, and they localized the monophosphorylation site to Ser118 (Fig. 5*C*, supplemental Figs. S14 and S15, and supplementary text). Thus, our top-down MS/MS data unambiguously confirmed that the proteoform with an M_r of 25,905.42 was the monophosphorylated form of swine ENH2 (Fig. 4*D*).

DISCUSSION

Concerted Reduction in the Phosphorylation of Myofilament and Z-disc Proteins—The PTM of myofilament proteins is increasingly recognized as an important mechanism for the

FIG. 4. **High-resolution MS for qualitative and quantitative analysis of myofilament and associated protein proteoforms.** *A–D*, representative high-resolution spectra of cTnI (*A*), MLC2 (*B*), Tm (*C*), and ENH2 (*D*) from CON (*top*) and AMI (*bottom*) myocardium. Circles represent the theoretical isotopic abundance distribution of the isotopomer peaks corresponding to the assigned mass. Single and double ellipses represent single and double oxidations, respectively. Stars represent non-covalent phosphoric acid adducts. *E*, relative quantification of cTnI, Tm, MLC2, and ENH2 protein proteoforms. All measurements were performed on three animals per group. Each biological replicate was performed in two technical replicates. Boxes, median and interquartile range (25%, 75%); whiskers, minimum and maximum values. $^*p < 0.05$, $^{**}p < 0.001$.

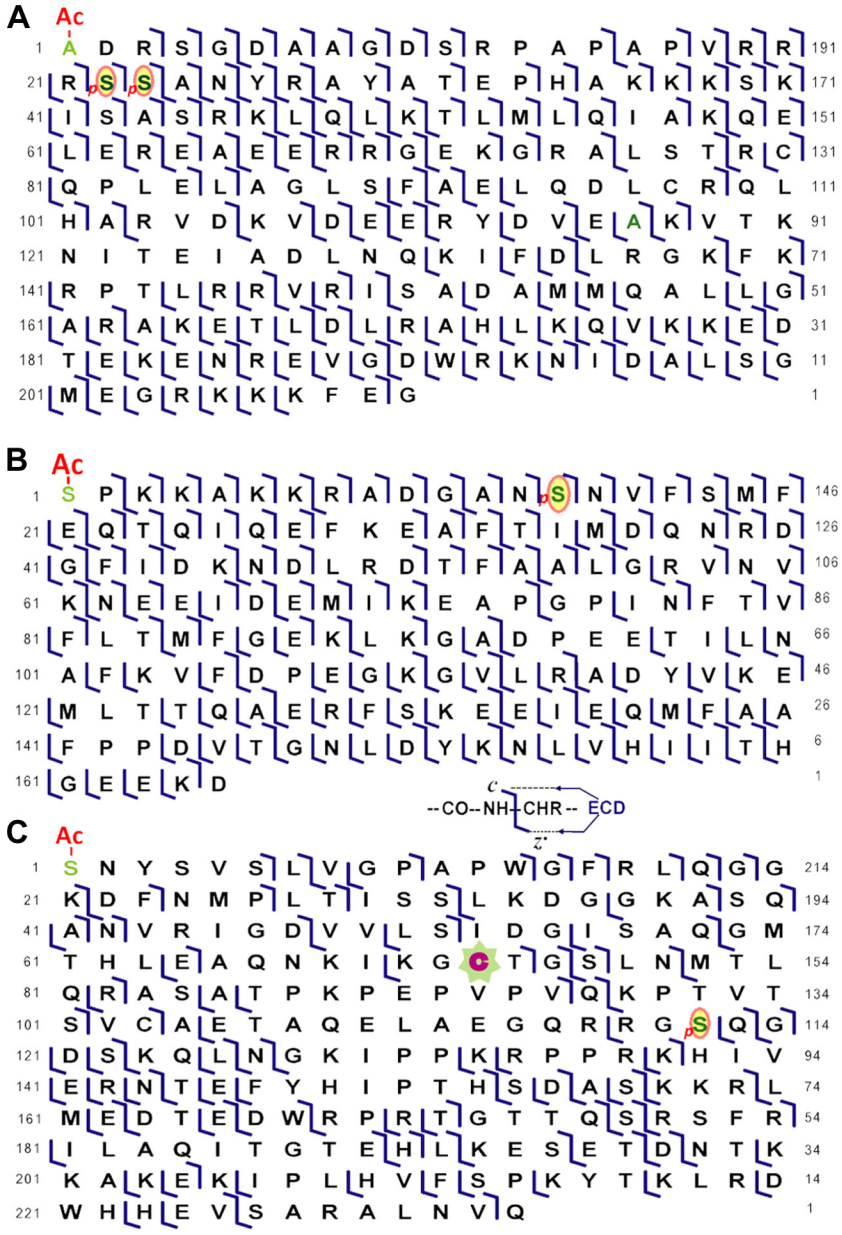

FIG. 5. **Comprehensive sequencing via ECD pinpointed the phosphorylation sites of $_{pp}$cTnI at Ser22/23 (*A*), $_{p}$MLC2 at Ser14 (*B*), and $_{p}$ENH2 at Ser118 (*C*).** "Ac" represents acetylation, and subscript "*p*" denotes phosphorylation. Phosphorylation sites are highlighted by circles (*A*–*C*). Amino acid polymorphism (Ser72Cys) is highlighted in a heptagon (*C*).

regulation of cardiac function, which requires highly coordinated protein–protein interactions among myofilament proteins in the sarcomere (6, 7). An emerging concept is that the integrated action of kinases and phosphatases regulates protein phosphorylation and, thus, ultimately determines the activity and function of myofilament and associated proteins (6). Consequently, an imbalance of kinase and phosphatase activities could alter contractility and lead to cardiac dysfunction. Indeed, our study presents direct evidence of early changes in protein phosphorylation occurring with cardiac dysfunction in a clinically relevant large-animal AMI model. Specifically, we detected a concerted reduction in the phosphorylation of three critical proteins in the sarcomere: cTnI (a thin filament regulatory protein), MLC2 (a thick filament regulatory protein), and ENH2 (a Z-disc protein) (Fig. 4 and Fig. 6). Using top-down high-resolution MS, we unambiguously localized the phosphorylation sites in these three proteins (Fig. 5). Although previous studies have shown reduced phosphorylation in myofilament proteins such as cardiac myosin binding protein C, MLC2, and cTnI (5, 46), this is the first report on the concerted changes in phosphorylation between myofilament proteins and Z-disc protein. Z-discs, which demarcate the ends of sarcomeres, are sophisticated structures that cross-link the myofilaments into highly ordered three-dimensional lattices (Fig. 6) (27, 29). Recent compelling evidence clearly indicates that the Z-disc may serve as a nodal point for cardiac signaling and disease (27). Importantly, our results suggest that coordinated signaling be-

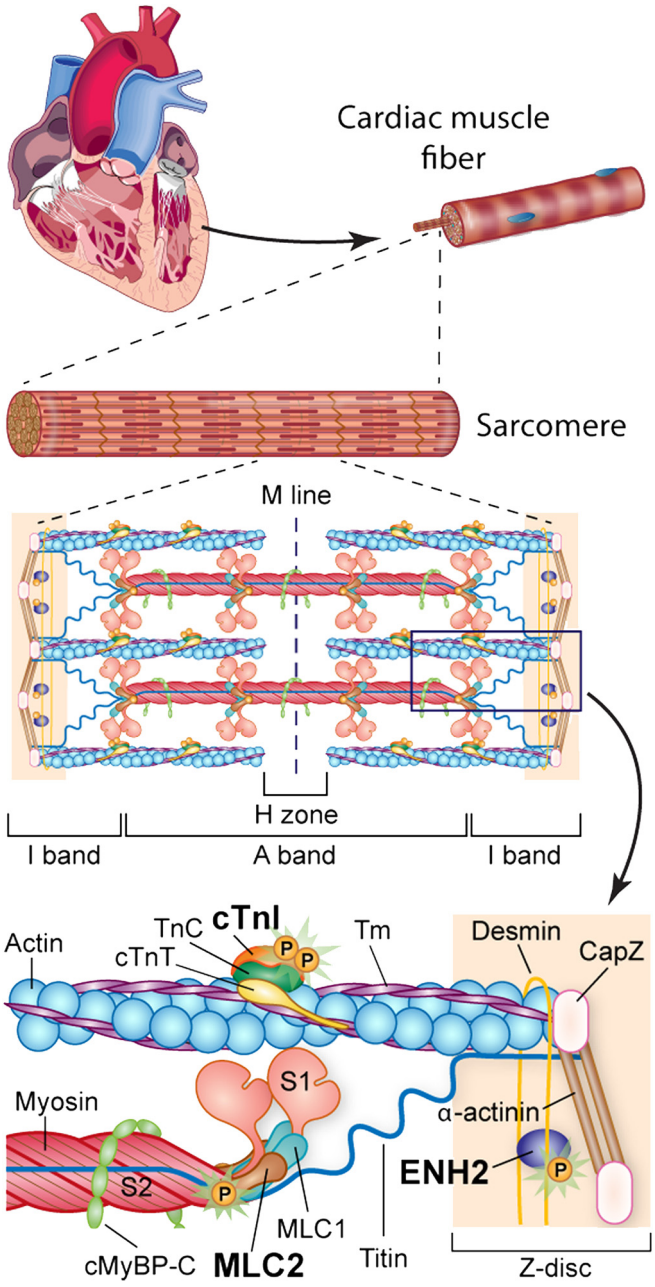

FIG. 6. **Schematic of myofilament and Z-disc proteins in the cardiac sarcomere with the phosphorylation of cTnI, MLC2, and ENH2 highlighted.** Only relevant proteins in the sarcomere, the basic contractile unit of cardiac muscle, are shown.

tween myofilament and Z-disc may underlie contractile dysfunction in AMI.

The Functional Significance of cTnI Phosphorylation at Ser22/23—Following stimulation of the β-adrenergic signaling system, activated PKA phosphorylates cTnI at residues Ser22/23, leading to decreased myofilament Ca^{2+} sensitivity and enhanced relaxation, which benefits diastolic function of the heart (40). We and others have previously reported that phosphorylation at Ser22/23 is significantly reduced in the human myocardium of end-stage HF patients relative to that of healthy donors (33, 47). In addition to PKA, other kinases such as PKC, cGMP-dependent protein kinase, and PKD can also cross-phosphorylate the PKA sites of cTnI at Ser22/23 and induce functional effects similar to those of PKA phosphorylation (40).

Previous reports by van der Velden *et al.* showed reduced cTnI phosphorylation and decreased PKA levels in the myocardium remote from the infarction in swine 3 weeks after MI in studies using open-chest LAD surgery (48). Avner *et al.* also reported the reduced phosphorylation of cTnI in the papillary muscles of mice 3 to 4 days after experimental MI via open-chest surgical ligation of the LAD (5). Importantly, in this study we observed significantly decreased cTnI phosphorylation immediately following 90 min of LAD occlusion using a closed-chest catheter-based method that obviates the need for open-chest surgery. Conceivably, a precise understanding of molecular changes at this early stage before the maladaptive remodeling could aid in the development of novel therapeutic interventions to prevent remodeling and the onset of HF.

The Functional Significance of MLC2 Phosphorylation—Here we observed reduced MLC2 phosphorylation within the infarction of acutely infarcted swine myocardium and unequivocally determined the predominant phosphorylation site to be Ser14. The decreased phosphorylation of MLC2 was also observed in human explanted end-stage failing hearts (49). Scruggs *et al.* determined the phosphorylation sites to be Ser13/14 (excluding the N-terminal Met) for mouse MLC2 and a single site at Ser14 for human MLC2 (50). Ser13 in mouse MLC2 is not conserved in the human sequence, but swine and human MLC2 have the same amino acid (Asn13) at this site; this underscores another advantage of the swine AMI model (supplemental Fig. S16). A recent study by Sheikh *et al.* demonstrated that knock-in mice with unphosphorylatable (S13A/S14A) MLC2 exhibit dilated cardiomyopathy, LV torsional defects, and sudden death, underlining the importance of MLC2 phosphorylation at Ser13/Ser14 (51).

The identity (or identities) of the kinase (or kinases) phosphorylating Ser14 of cardiac MLC2 remains unclear. Originally, MLC2 was presumed to be phosphorylated by MLC2 kinase (myosin light chain kinase) and dephosphorylated by MLC2 phosphatase (52). Although the conventional smooth and skeletal muscle myosin light chain kinases are also expressed in the heart, they do not appear to play a significant role in regulating MLC2 phosphorylation and altering cardiac function (43). Recently, a cardiac-specific MLC2 kinase (cardiac myosin light chain kinase) encoded by Mylk3 was shown to be the primary kinase phosphorylating MLC2 that modulates cardiac function in both mice and humans (53). Besides cardiac myosin light chain kinase, other kinases such as zipper-interacting protein kinase, rho-associated kinase, and PKC may also regulate MLC2 phosphorylation (43, 52).

ENH2 Phosphorylation and Cardiac Z-disc Signaling—ENH belongs to the PDZ-LIM domain protein family that co-localizes with α-actinin on the Z-disc (Fig. 6) and associates with cytoskeletal proteins through its PDZ domain (27, 28, 45). ENH is alternatively spliced into four isoforms: isoform 1 (ENH 1) is the long isoform containing a PDZ domain and three LIM domains, whereas the other three short isoforms (ENH2–ENH4) retain only the PDZ domain (45). ENH2, -3, and -4 are expressed mainly in cardiac and skeletal muscle, whereas ENH1 is ubiquitously expressed in all tissue types. The splicing isoforms of ENH are differentially expressed during heart development and disease (45). ENH1 appears to be the embryonic isoform, whereas the other isoforms are predominant in adult heart (45). Recently, Chen and co-workers found that ENH-null mice develop impaired cardiac contraction and dilated cardiomyopathy, underscoring the critical role of ENH in the heart (28). The loss of ENH likely perturbs the integrity of the Z-disc, thus disturbing the connection between adjacent sarcomeres and the extracellular milieu (28).

Here we show that ENH2 is a phosphoprotein with a phosphorylation site at Ser118; however, the functional significance of this phosphorylation remains to be investigated. PDZ-LIM proteins typically serve as adaptor proteins in the Z-disc: the PDZ domain mediates interactions with the cytoskeleton, and the LIM domain recruits signaling proteins to the Z-disc. The perception of the cardiac Z-disc has changed considerably in the past decade (27, 29, 30). Traditionally the Z-disc was only viewed as a structural component in the sarcomere, but recent compelling evidence clearly indicates that the Z-disc may serve as a hub for cardiac signaling and disease (27). An increasing number of signaling proteins, including protein kinases and phosphatases, are co-localized to the Z-disc, thereby concentrating a number of intracellular signaling molecules in this specific subcellular location (27). Notably, for the first time, we discovered the phosphorylation of a critical Z-disc protein, ENH2, and its down-regulation after 90 min of ischemia, suggesting pivotal roles for this protein phosphorylation and the Z-disc in pathological signaling after AMI.

Top-down Quantitative Proteomics Reveals Concerted and Unexpected Proteoform Changes—We have successfully developed a novel LC/MS-based top-down proteomics strategy for the highly reproducible quantification of multiple proteoforms simultaneously (Fig. 1). There are several major advantages of this strategy. The first is rapid and effective separation of intact key cardiac proteins in the myofilament subproteome extracted from tissues. Here we have shown that a majority of lower mass ($<$60 kDa) proteins from myofilaments and their associated proteins can be fully or partially separated on an LC time scale (Fig. 2, supplemental Fig. S6). A minimal amount of tissue ($\sim$500 μg per experiment) is sufficient for both LC/MS and high-resolution MS characterization of proteins, making it suitable for the analysis of human biopsy samples. The approach also allows global detection of all types of modifications simultaneously without *a priori* knowledge. The antibody-based methods for detecting PTMs (*i.e.* Western blot) require prior knowledge of the modification. In the conventional bottom-up MS approach, proteins are digested extensively with an enzyme (*e.g.* trypsin), resulting in many small peptides for MS and MS/MS analysis. This bottom-up approach is particularly useful for identifying proteins, but it is suboptimal for determining modifications and alternative splice variants because of the partial recovery of digested peptides, which can result in missed identification of PTMs and a loss of connectivity between different modifications (54). In contrast, a top-down MS approach analyzes whole proteins without digestion, thus providing a comprehensive view of the protein (18, 55, 56). Therefore, top-down MS is the only technique that can simultaneously identify all types of protein modifications universally without *a priori* knowledge. Here, we employed top-down MS to reveal a variety of proteoforms for myofilament and associated proteins arising from PTMs (*i.e.* phosphorylation, degradation, oxidation, acetylation), polymorphism, and alternatively spliced isoforms (Fig. 4). Another advantage is the comprehensive sequencing and identification of (unexpected) modifications. In the top-down MS approach, the molecular masses of the intact proteins are measured in the first step, which can reveal any modifications occurring to the proteins, including unexpected ones (18). Subsequently, proteoforms of interest can be isolated and fragmented via MS/MS with ECD and CAD to locate the (unexpected) modification sites (57–59). Here we have comprehensively sequenced cTnI, MLC2, and ENH2 (Fig. 5, supplemental Figs. S9–S11) and mapped unexpected modifications, as exemplified by an amino acid polymorphism and phosphorylation for ENH2 (Fig. 5*C*, supplemental Fig. S14). The use of ECD particularly allows for the localization of labile PTMs such as phosphorylation with high reliability and accuracy (12, 18, 25, 32, 33, 60). We localized Ser22/23 as the phosphorylation sites for cTnI, Ser14 as the phosphorylation site in MLC2, and an unexpected phosphorylation site, Ser118, in ENH2. The identification of unexpected modifications is challenging in the bottom-up approach, as typically modifications need to be defined prior to a database search for the identification of such modifications. Our approach also permits the quantification of protein proteoforms with high reproducibility and identification of concerted changes in responding to pathophysiological stimuli. The addition of small modifying groups to intact proteins does not change the physiochemical properties (and thus the ionization efficiency of proteins) appreciably, in contrast to the dramatic impact such modifying groups could have on the ionization efficiency of small peptides (25, 61, 62). Moreover, the phosphorylation of a protein has a minimal influence on the protein charge state distribution (supplemental Fig. S17). Thus, top-down MS is the method of choice for the quantification of various protein proteoforms. We have achieved remarkable reproducibility with this top-

down quantitative proteomics method (supplemental Figs. S4 and S5), and we reliably quantified various proteoforms and determined the changes following AMI (Fig. 4). Appreciably, we have unambiguously identified the reduction of phosphorylation in cTnI (a thin filament regulatory protein), MLC2 (a thick filament regulatory protein), and ENH2 (a Z-disc protein) after AMI. Finally, the current approach employs a combination of on-line low-resolution LC/MS for rapid profiling and off-line high-resolution MS for comprehensive proteoform characterization. We employed an "LC/MS+" platform that allows fraction collection concurrent with on-line LC/MS, previously known as a "data-directed top-down" approach (63–65). The on-line low-resolution LC/MS provides rapid screening of potential proteoform changes, which can then guide user-directed data-dependent high-resolution top-down MS experiments. The fractions collected simultaneously during the on-line LC/MS are used for comprehensive sequence characterization and accurate proteoform quantification. Thus, this targeted top-down proteomics approach offers the benefits of high-throughput protein profiling, high-resolution protein characterization, and high-accuracy quantification of proteoforms from a subproteome.

The potential limitation of our one-dimensional LC/MS-based top-down quantitative proteomics method is its failure to detect large myofilament and associated proteins such as α-actinin (~110 kDa), cardiac myosin binding protein C (~140 kDa), and myosin heavy chain (~220 kDa), which are known to be present in the myofilament subproteome in the cardiac sarcomere (Fig. 6). Because of the exponential decay in the signal-to-noise ratio as a function of increasing mass, it is necessary to separate the small molecules from large proteins (66). For instance, we could use two-dimensional LC with size exclusion chromatography as the first dimension and reverse phase chromatography as the second dimension. We have recently shown that ultra-high-pressure size exclusion chromatography can be used for the rapid and high-resolution separation of intact proteins for top-down proteomics (67). Nevertheless, two-dimensional LC typically requires longer sample analysis times, so caution should be taken to minimize the possible artifactual modifications.

In summary, we have developed a novel LC/MS-based top-down quantitative proteomics strategy to comprehensively assess the changes in key cardiac proteins present in the myofilament subproteome extracted from heart tissues with high reproducibility and throughput. This entire process, which includes tissue homogenization, protein extraction, and on-line LC/MS analysis, takes less than 3 h and requires a minimal amount of myocardial tissue (~500 μg of tissue per experiment), making it possible to analyze biopsy samples routinely. Enabled by this top-down quantitative proteomics strategy and a highly clinically relevant large-animal (swine) model, we have unveiled the molecular changes of the critical cardiac proteins in the myofilaments and Z-disc at the early stage after AMI. Our proteomics discovery opens up new avenues for further investigation of the potential link between myofilament and Z-disc in regulating cardiac contractility at the early stage post-MI that might lead to maladaptive remodeling and ultimately HF.

Acknowledgments—We thank Matthew Lawrence and Chad Dooley for technical assistance during the early stage of this project. We also thank Wei Guo and Serife Ayaz-Guner for helpful discussions and critical reading of this manuscript.

* Financial support was kindly provided by NIH R01HL096971 and R01HL109810 (to Y.G.). Y.G. acknowledges American Heart Association Scientist Development Grant 0735443Z and the Wisconsin Partnership Fund for the establishment of the Human Proteomics Program Mass Spectrometry Facility.

S This article contains supplemental material.

|||| To whom correspondence should be addressed: Dr. Ying Ge, 1300 University Ave., SMI 130, Madison, WI 53706. Tel.: 608-263-9212; Fax: 608-265-5512; E-mail: ge2@wisc.edu.

REFERENCES

1. de Couto, G., Ouzounian, M., and Liu, P. P. (2010) Early detection of myocardial dysfunction and heart failure. *Nat. Rev. Cardiol.* **7,** 334–344
2. Roger, V. L., Go, A. S., Lloyd-Jones, D. M., Benjamin, E. J., Berry, J. D., Borden, W. B., Bravata, D. M., Dai, S., Ford, E. S., Fox, C. S., Fullerton, H. J., Gillespie, C., Hailpern, S. M., Heit, J. A., Howard, V. J., Kissela, B. M., Kittner, S. J., Lackland, D. T., Lichtman, J. H., Lisabeth, L. D., Makuc, D. M., Marcus, G. M., Marelli, A., Matchar, D. B., Moy, C. S., Mozaffarian, D., Mussolino, M. E., Nichol, G., Paynter, N. P., Soliman, E. Z., Sorlie, P. D., Sotoodehnia, N., Turan, T. N., Virani, S. S., Wong, N. D., Woo, D., Turner, M. B., American Heart Association Statistics Committee, and Stroke Statistics Subcommittee (2012) Executive summary: heart disease and stroke statistics—2012 update: a report from the American Heart Association. *Circulation* **125,** 188–197
3. Mudd, J. O., and Kass, D. A. (2008) Tackling heart failure in the twenty-first century. *Nature* **451,** 919–928
4. Pfeffer, M. A., and Braunwald, E. (1990) Ventricular remodeling after myocardial infarction. Experimental observations and clinical implications. *Circulation* **81,** 1161–1172
5. Avner, B. S., Shioura, K. M., Scruggs, S. B., Grachoff, M., Geenen, D. L., Helseth, D. L., Jr., Farjah, M., Goldspink, P. H., and Solaro, R. J. (2012) Myocardial infarction in mice alters sarcomeric function via post-translational protein modification. *Mol. Cell. Biochem.* **363,** 203–215
6. Yuan, C., and Solaro, R. J. (2008) Myofilament proteins: from cardiac disorders to proteomic changes. *Proteomics Clin. Appl.* **2,** 788–799
7. Jin, W. H., Brown, A. T., and Murphy, A. M. (2008) Cardiac myofilaments: from proteome to pathophysiology. *Proteomics Clin. Appl.* **2,** 800–810
8. Solaro, R. J., Warren, C. M., and Scruggs, S. B. (2010) Why is it important to analyze the cardiac sarcomere subproteome? *Expert Rev. Proteomics* **7,** 311–314
9. Solaro, R. J. (2008) Multiplex kinase signaling modifies cardiac function at the level of sarcomeric proteins. *J. Biol. Chem.* **283,** 26829–26833
10. Moss, R. L., Razumova, M., and Fitzsimons, D. P. (2004) Myosin cross-bridge activation of cardiac thin filaments—implications for myocardial function in health and disease. *Circ. Res.* **94,** 1290–1300
11. Takeda, S., Yamashita, A., Maeda, K., and Maeda, Y. (2003) Structure of the core domain of human cardiac troponin in the Ca^{2+}-saturated form. *Nature* **424,** 35–41
12. Ge, Y., Rybakova, I. N., Xu, Q., and Moss, R. L. (2009) Top-down high-resolution mass spectrometry of cardiac myosin binding protein C revealed that truncation alters protein phosphorylation state. *Proc. Natl. Acad. Sci. U.S.A.* **106,** 12658–12663
13. Yin, X., Cuello, F., Mayr, U., Hao, Z., Hornshaw, M., Ehler, E., Avkiran, M., and Mayr, M. (2010) Proteomics analysis of the cardiac myofilament subproteome reveals dynamic alterations in phosphatase subunit distribution. *Mol. Cell. Proteomics* **9,** 497–509
14. Han, X. M., Jin, M., Breuker, K., and McLafferty, F. W. (2006) Extending top-down mass spectrometry to proteins with masses greater than 200 kilodaltons. *Science* **314,** 109–112

15. Ge, Y., Lawhorn, B. G., ElNaggar, M., Strauss, E., Park, J. H., Begley, T. P., and McLafferty, F. W. (2002) Top down characterization of larger proteins (45 kDa) by electron capture dissociation mass spectrometry. *J. Am. Chem. Soc.* **124,** 672–678
16. Kelleher, N. L., Lin, H. Y., Valaskovic, G. A., Aaserud, D. J., Fridriksson, E. K., and McLafferty, F. W. (1999) Top down versus bottom up protein characterization by tandem high-resolution mass spectrometry. *J. Am. Chem. Soc.* **121,** 806–812
17. Siuti, N., and Kelleher, N. L. (2007) Decoding protein modifications using top-down mass spectrometry. *Nat. Methods* **4,** 817–821
18. Zhang, H., and Ge, Y. (2011) Comprehensive analysis of protein modifications by top-down mass spectrometry. *Circ. Cardiovasc. Genet.* **4,** 711
19. Tran, J. C., Zamdborg, L., Ahlf, D. R., Lee, J. E., Catherman, A. D., Durbin, K. R., Tipton, J. D., Vellaichamy, A., Kellie, J. F., Li, M., Wu, C., Sweet, S. M., Early, B. P., Siuti, N., LeDuc, R. D., Compton, P. D., Thomas, P. M., and Kelleher, N. L. (2011) Mapping intact protein isoforms in discovery mode using top-down proteomics. *Nature* **480,** 254–258
20. Ansong, C., Wu, S., Meng, D., Liu, X., Brewer, H. M., Deatherage Kaiser, B. L., Nakayasu, E. S., Cort, J. R., Pevzner, P., Smith, R. D., Heffron, F., Adkins, J. N., and Pasa-Tolic, L. (2013) Top-down proteomics reveals a unique protein S-thiolation switch in Salmonella typhimurium in response to infection-like conditions. *Proc. Natl. Acad. Sci. U.S.A.* **110,** 10153–10158
21. Peng, Y., Chen, X., Zhang, H., Xu, Q., Hacker, T. A., and Ge, Y. (2013) Top-down targeted proteomics for deep sequencing of tropomyosin isoforms. *J. Proteome Res.* **12,** 187–198
22. Ryan, C. M., Souda, P., Bassilian, S., Ujwal, R., Zhang, J., Abramson, J., Ping, P., Durazo, A., Bowie, J. U., Hasan, S. S., Baniulis, D., Cramer, W. A., Faull, K. F., and Whitelegge, J. P. (2010) Post-translational modifications of integral membrane proteins resolved by top-down Fourier transform mass spectrometry with collisionally activated dissociation. *Mol. Cell. Proteomics* **9,** 791–803
23. Smith, L. M., and Kelleher, N. L. (2013) Proteoform: a single term describing protein complexity. *Nat. Methods* **10,** 186–187
24. Zubarev, R. A., Horn, D. M., Fridriksson, E. K., Kelleher, N. L., Kruger, N. A., Lewis, M. A., Carpenter, B. K., and McLafferty, F. W. (2000) Electron capture dissociation for structural characterization of multiply charged protein cations. *Anal. Chem.* **72,** 563–573
25. Zabrouskov, V., Ge, Y., Schwartz, J., and Walker, J. W. (2008) Unraveling molecular complexity of phosphorylated human cardiac troponin I by top down electron capture dissociation/electron transfer dissociation mass spectrometry. *Mol. Cell. Proteomics* **7,** 1838–1849
26. Tomkowiak, M. T., Klein, A. J., Vigen, K. K., Hacker, T. A., Speidel, M. A., VanLysel, M. S., and Raval, A. N. (2011) Targeted transendocardial therapeutic delivery guided by MRI-X-ray image fusion. *Catheter Cardiovasc. Intervent.* **78,** 468–478
27. Wang, X., and Su, H. (2010) Unraveling enigma in the Z-disk. *Circ. Res.* **107,** 321–323
28. Cheng, H., Kimura, K., Peter, A. K., Cui, L., Ouyang, K., Shen, T., Liu, Y., Gu, Y., Dalton, N. D., Evans, S. M., Knowlton, K. U., Peterson, K. L., and Chen, J. (2010) Loss of enigma homolog protein results in dilated cardiomyopathy. *Circulation* **107,** 348–356
29. Pyle, W. G., and Solaro, R. J. (2004) At the crossroads of myocardial signaling—the role of Z-discs in intracellular signaling and cardiac function. *Circ. Res.* **94,** 296–305
30. Frank, D., and Frey, N. (2011) Cardiac Z-disc signaling network. *J. Biol. Chem.* **286,** 9897–9904
31. Neverova, I., and Van Eyk, J. E. (2002) Application of reversed phase high performance liquid chromatography for subproteomic analysis of cardiac muscle. *Proteomics* **2,** 22–31
32. Dong, X., Sumandea, C. A., Chen, Y.-C., Garcia-Cazarin, M. L., Zhang, J., Balke, C. W., Sumandea, M. P., and Ge, Y. (2012) Augmented phosphorylation of cardiac troponin I in hypertensive heart failure. *J. Biol. Chem.* **287,** 848–857
33. Zhang, J., Guy, M. J., Norman, H. S., Chen, Y.-C., Xu, Q., Dong, X., Guner, H., Wang, S., Kohmoto, T., Young, K. H., Moss, R. L., and Ge, Y. (2011) Top-down quantitative proteomics identified phosphorylation of cardiac troponin I as a candidate biomarker for chronic heart failure. *J. Proteome Res.* **10,** 4054–4065
34. Guner, H., Close, P. L., Cai, W., Zhang, H., Peng, Y., Chen, Y., Gregorich, Z. R., and Ge, Y. (2014) MASH suite: a user-friendly and versatile software interface for high-resolution mass spectrometry data interpretation and visualization. *J. Am. Soc. Mass Spectrom.* **25,** 464–470
35. Liu, X., Inbar, Y., Dorrestein, P. C., Wynne, C., Edwards, N., Souda, P., Whitelegge, J. P., Bafna, V., and Pevzner, P. A. (2010) Deconvolution and database search of complex tandem mass spectra of intact proteins. *Mol. Cell. Proteomics* **9,** 2772–2782
36. Liu, X. W., Sirotkin, Y., Shen, Y. F., Anderson, G., Tsai, Y. S., Ting, Y. S., Goodlett, D. R., Smith, R. D., Bafna, V., and Pevzner, P. A. (2012) Protein identification using top-down. *Mol. Cell. Proteomics* **11,** M111.008524
37. Peng, Y., Yu, D. Y., Gregorich, Z., Chen, X., Beyer, A. M., Gutterman, D. D., and Ge, Y. (2013) In-depth proteomic analysis of human tropomyosin by top-down mass spectrometry. *J. Muscle Res. Cell Motil.* **34,** 199–210
38. Dixon, J. A., and Spinale, F. G. (2009) Large animal models of heart failure: a critical link in the translation of basic science to clinical practice. *Circ. Heart Fail.* **2,** 262–271
39. Vilahur, G., Juan-Babot, O., Pena, E., Onate, B., Casani, L., and Badimon, L. (2011) Molecular and cellular mechanisms involved in cardiac remodeling after acute myocardial infarction. *J. Mol. Cell. Cardiol.* **50,** 522–533
40. Layland, J., Solaro, R. J., and Shah, A. M. (2005) Regulation of cardiac contractile function by troponin I phosphorylation. *Cardiovasc. Res.* **66,** 12–21
41. Solaro, R. J., Henze, M., and Kobayashi, T. (2013) Integration of troponin I phosphorylation with cardiac regulatory networks. *Circ. Res.* **112,** 355–366
42. Solaro, R. J., and van der Velden, J. (2010) Why does troponin I have so many phosphorylation sites? Fact and fancy. *J. Mol. Cell. Cardiol.* **48,** 810–816
43. Sheikh, F., Lyon, R. C., and Chen, J. (2014) Getting the skinny on thick filament regulation in cardiac muscle biology and disease. *Trends Cardiovasc. Med.* **24,** 133–141
44. Moss, R. L., and Fitzsimons, D. P. (2006) Myosin light chain 2 into the mainstream of cardiac development and contractility. *Circ. Res.* **99,** 225–227
45. Yamazaki, T., Walchli, S., Fujita, T., Ryser, S., Hoshijima, M., Schlegel, W., Kuroda, S. i., and Maturana, A. D. (2010) Splice variants of Enigma homolog, differentially expressed during heart development, promote or prevent hypertrophy. *Cardiovasc. Res.* **86,** 374–382
46. El-Armouche, A., Pohlmann, L., Schlossarek, S., Starbatty, J., Yeh, Y. H., Nattel, S., Dobrev, D., Eschenhagen, T., and Carrier, L. (2007) Decreased phosphorylation levels of cardiac myosin-binding protein-C in human and experimental heart failure. *J. Mol. Cell. Cardiol.* **43,** 223–229
47. Messer, A. E., Jacques, A. M., and Marston, S. B. (2007) Troponin phosphorylation and regulatory function in human heart muscle: dephosphorylation of Ser23/24 on troponin I could account for the contractile defect in end-stage heart failure. *J. Mol. Cell. Cardiol.* **42,** 247–259
48. van der Velden, J., Merkus, D., Klarenbeek, B. R., James, A. T., Boontje, N. M., Dekkers, D. H. W., Stienen, G. J. M., Lamers, J. M. J., and Duncker, D. J. (2004) Alterations in myofilament function contribute to left ventricular dysfunction in pigs early after myocardial infarction. *Circ. Res.* **95,** E85–E104
49. van der Velden, J., Papp, Z., Boontje, N. M., Zaremba, R., de Jong, J. W., Janssen, P. M. L., Hasenfuss, G., and Stienen, G. J. M. (2003) The effect of myosin light chain 2 dephosphorylation on Ca^{2+}-sensitivity of force is enhanced in failing human hearts. *Cardiovasc. Res.* **57,** 505–514
50. Scruggs, S. B., Reisdorph, R., Armstrong, M. L., Warren, C. M., Reisdorph, N., Solaro, R. J., and Buttrick, P. M. (2010) A novel, in-solution separation of endogenous cardiac sarcomeric proteins and identification of distinct charged variants of regulatory light cChain. *Mol. Cell. Proteomics* **9,** 1804–1818
51. Sheikh, F., Ouyang, K., Campbell, S. G., Lyon, R. C., Chuang, J., Fitzsimons, D., Tangney, J., Hidalgo, C. G., Chung, C. S., Cheng, H., Dalton, N. D., Gu, Y., Kasahara, H., Ghassemian, M., Omens, J. H., Peterson, K. L., Granzier, H. L., Moss, R. L., McCulloch, A. D., and Chen, J. (2012) Mouse and computational models link Mlc2v dephosphorylation to altered myosin kinetics in early cardiac disease. *J. Clin. Invest.* **122,** 1209–1221
52. Scruggs, S. B., and Solaro, R. J. (2011) The significance of regulatory light chain phosphorylation in cardiac physiology. *Arch. Biochem. Biophys.* **510,** 129–134
53. Chan, J. Y., Takeda, M., Briggs, L. E., Graham, M. L., Lu, J. T., Horikoshi, N., Weinberg, E. O., Aoki, H., Sato, N., Chien, K. R., and Kasahara, H.

(2008) Identification of cardiac-specific myosin light chain kinase. *Circ. Res.* **102,** 571–580
54. Chait, B. T. (2006) Mass spectrometry: bottom-up or top-down? *Science* **314,** 65–66
55. Gregorich, Z. R., and Ge, Y. (2014) Top-down proteomics in health and disease: challenges and opportunities. *Proteomics* **14,** 1195–1210
56. Tipton, J. D., Tran, J. C., Catherman, A. D., Ahlf, D. R., Durbin, K. R., and Kelleher, N. L. (2011) Analysis of intact protein isoforms by mass spectrometry. *J. Biol. Chem.* **286,** 25451–25458
57. Zhang, J., Dong, X., Hacker, T. A., and Ge, Y. (2010) Deciphering modifications in swine cardiac troponin I by top-down high-resolution tandem mass spectrometry. *J. Am. Soc. Mass Spectrom.* **21,** 940–948
58. Kuhn, P., Xu, Q., Cline, E., Zhang, D., Ge, Y., and Xu, W. (2009) Delineating Anopheles gambiae coactivator associated arginine methyltransferase 1 automethylation using top-down high resolution tandem mass spectrometry. *Protein Sci.* **18,** 1272–1280
59. Sze, S. K., Ge, Y., Oh, H., and McLafferty, F. W. (2002) Top-down mass spectrometry of a 29-kDa protein for characterization of any posttranslational modification to within one residue. *Proc. Natl. Acad. Sci. U.S.A.* **99,** 1774–1779
60. Ayaz-Guner, S., Zhang, J., Li, L., Walker, J. W., and Ge, Y. (2009) In vivo phosphorylation site mapping in mouse cardiac troponin I by high resolution top-down electron capture dissociation mass spectrometry: Ser22/23 are the only sites basally phosphorylated. *Biochemistry* **48,** 8161–8170
61. Pesavento, J. J., Mizzen, C. A., and Kelleher, N. L. (2006) Quantitative analysis of modified proteins and their positional isomers by tandem mass spectrometry: human histone H4. *Anal Chem* **78,** 4271–4280
62. Pesavento, J. J., Bullock, C. R., LeDuc, R. D., Mizzen, C. A., and Kelleher, N. L. (2008) Combinatorial modification of human histone H4 quantitated by two-dimensional liquid chromatography coupled with top down mass spectrometry. *J. Biol. Chem.* **283,** 14927–14937
63. Thangaraj, B., Ryan, C. M., Souda, P., Krause, K., Faull, K. F., Weber, A. P. M., Fromme, P., and Whitelegge, J. P. (2010) Data-directed top-down Fourier-transform mass spectrometry of a large integral membrane protein complex: Photosystem II from Galdieria sulphuraria. *Proteomics* **10,** 3644–3656
64. Souda, P., Ryan, C. M., Cramer, W. A., and Whitelegge, J. (2011) Profiling of integral membrane proteins and their post translational modifications using high-resolution mass spectrometry. *Methods* **55,** 330–336
65. Whitelegge, J., Halgand, F., Souda, P., and Zabrouskov, V. (2006) Top-down mass spectrometry of integral membrane proteins. *Expert Rev. Proteomics* **3,** 585–596
66. Compton, P. D., Zamdborg, L., Thomas, P. M., and Kelleher, N. L. (2011) On the scalability and requirements of whole protein mass spectrometry. *Anal. Chem.* **83,** 6868–6874
67. Chen, X., and Ge, Y. (2013) Ultrahigh pressure fast size exclusion chromatography for top-down proteomics. *Proteomics* **13,** 2563–2566